Statistical Interconnect Metrics for Physical-Design Optimization

Kanak Agarwal, *Member, IEEE*, Mridul Agarwal, Dennis Sylvester, *Senior Member, IEEE*, and David Blaauw, *Member, IEEE*

***Abstract*—In this paper, statistical models for the efficient analysis of interconnect delay and crosstalk noise in the presence of back-end process variations are developed. The proposed models enable closed-form computation of means and variances of interconnect-delay, crosstalk-noise peak, and coupling-induced-delay change for given magnitudes of variation in relevant process parameters, such as linewidth, metal thickness, metal spacing, and interlayer dielectric (ILD) thickness. The proposed approach is based on the observation that if the variations in different physical dimensions are assumed to be independent normal random variables, then the interconnect behavior also tends to have a Gaussian distribution. In the proposed statistical models, delay and noise are expressed directly as functions of changes in physical parameters. This formulation allows us to preserve all correlations and can be very useful in evaluating delay and noise sensitivities due to changes in various physical dimensions. For interconnect-delay computation, the authors express the resistance and capacitance of a line as a linear function of random variables and then use these to compute circuit moments. They show that ignoring higher order terms in the resulting variational moments does not result in a loss of accuracy. Finally, these variability-aware moments are used in known closed-form delay and slew metrics to compute interconnect-delay probability density functions (pdfs). Similarly for coupling noise and dynamic-delay analysis, the authors rely on the linearity (Gaussian) assumption, allowing us to truncate nonlinear terms and express noise and dynamic-delay pdfs as linear functions of variations in relevant geometric dimensions. They compare their approach to SPICE-based Monte Carlo simulations and report the error in mean and standard deviation of interconnect delay to be 1% and 4% on average, respectively.**

***Index Terms*—Coupling, crosstalk noise, delay metric, integrated circuit interconnect, process variation, RC trees, slew, statistical modeling, timing analysis.**

I. Introduction

With process technologies shrinking to the nanometer regime, the impact of process variation on performance has become extremely critical [1]–[3]. Manufacturing variations can be random in nature and cause significant discrepancies between the designed and the manufactured products. The importance of these variations is increasing rapidly with the scaling of design dimensions. This is true since process tolerances do not scale proportionally with the design dimensions, causing the relative impact of the process variations to increase with every new technology generation [4]. Hence, it is now vital that manufacturing variations be included within timing analyses.

In addition to influencing timing, process variations also impact signal-integrity issues such as crosstalk noise, coupling-induced delay, electromigration, IR drop, etc. When process variations impact these parameters significantly, manufactured products may experience unexpected reliability failures. Therefore, it is extremely important to include variability during reliability analysis and optimization—this will minimize yield loss due to reliability failures caused by process variation and ensure a robust design across the entire process spread.

Process variation can significantly impact both device (front end of the line) and interconnect (back end of the line) performance [5]. In this work, we focus on modeling the impact of process variation on interconnect performance. The effects of device-parameter variations are typically captured using a corner-based analysis (based on the understanding that smaller channel lengths always yield faster circuits, etc.). However, it has been shown that corner-based analysis cannot be applied to interconnect due to their context-dependent nature [6]. In particular, for two different interconnect structures, when metal thickness is increased, the delay of one structure can increase, while that of the other structure may decrease [6]. This makes it difficult to capture the impact of variability on interconnect delay using traditional corner-based methods.

Recently, work was proposed to capture the effect of interconnect variability on timing. Liu *et al.* [7] proposes a reduced-order modeling approach that includes manufacturing variations. The authors suggest a mathematical framework to perform variational analysis using model-order-reduction techniques such as the passive reduced-order interconnect macromodeling algorithm (PRIMA) [8]. However, the proposed approach is computationally expensive due to the lack of closed-form expressions. A second drawback of the approach is that it can only be used to predict the change in interconnect delay due to deterministic values of the changes in the physical dimensions. In reality, changes in physical dimensions are not deterministic values but are random variables. Therefore, it is required that an interconnect analysis framework be developed that takes in probability density functions (pdfs) of the changes in physical dimensions and outputs the pdf of the change in the interconnect delay. In this paper, we propose a methodology to achieve this objective.

This type of new interconnect-modeling approach must be computationally efficient in order to be useful in incremental

Manuscript received August 30, 2004; revised January 10, 2005. This work was supported by a Grant from National Science Foundation (NSF). This paper was recommended by Associate Editor C. J. Alpert.

K. Agarwal, D. Sylvester, and D. Blaauw are with the Department of Electrical Engineering and Computer Science, University of Michigan, Ann Arbor, MI 48109 USA (e-mail: kba@us.ibm.com).

M. Agarwal is with the Department of Electrical Engineering, Indian Institute of Technology, Kanpur, India.

Digital Object Identifier 10.1109/TCAD.2005.855954

0278-0070/$20.00 © 2006 IEEE

Authorized licensed use limited to: University of Michigan Library. Downloaded on November 14, 2008 at 14:44 from IEEE Xplore. Restrictions apply.

timing analysis and physical-design optimizations. This same requirement has led to substantial recent effort in developing closed-form metrics for nominal interconnect-delay calculation. Several of these metrics are briefly discussed in the next section as background. In this paper, we incorporate variability into these metrics and propose the use of closed-form variational-delay metrics that can be used to efficiently predict the mean and variance of interconnect delay in the presence of uncertainty in the geometric dimensions. We also show that delay pdfs due to wiring variability are nearly Gaussian. This has the added advantage that if the mean and the variance of the delay pdf can be computed efficiently, then any confidence point in the delay calculation can be easily predicted.

Besides statistical-interconnect-delay analysis, we also analyze the impact of interconnect variations on signal-integrity issues, such as crosstalk noise and coupling-induced-delay degradation (i.e., dynamic delay). Accurate statistical modeling of interconnect coupling requires accurate nominal models for crosstalk noise and coupling-induced-delay change caused by the simultaneous switching of aggressor and victim wires. Modeling static noise has been a heavily studied topic and various static-noise models have been proposed that exhibit a high degree of accuracy [9]–[14]. On the other hand, accurate estimation of crosstalk-induced delay remains a challenging task. Typically, dynamic delay is modeled by replacing the coupling capacitance between two wires by an equivalent ground capacitance based on the Miller effect [15]. A few other approaches model dynamic delay by the superposition of a static-noise waveform on the nominal switching waveform of the isolated victim [16], [17]. These superposition-based approaches require accurate modeling of static noise and nominal victim waveforms. These waveforms must then be properly aligned to obtain worst case delay change [18]. In this work, we develop a new nominal closed-form dynamic-delay model that uses advanced waveform models such as Weibull, along with worst case alignment, to obtain peak-crosstalk-induced delay degradation. This new model, along with existing static noise and delay models, is then used to obtain statistical models of coupling effects under interconnect variations. By using our model, the means and variances of the static-noise peak and the worst case crosstalk noise can be expressed in closed-form expressions, thereby making the proposed analysis useful in statistical noise-related physical-design optimizations.

The remainder of this paper is organized as follows. In Section II, we propose a new approach for variational-delay metrics. Sections III and IV discuss the statistical modeling of static noise and dynamic delay, respectively. We then present our results in Section V, before concluding in Section VI.

II. Variational Interconnect-Timing Metrics

In this section, we develop variational delay metrics for statistical-interconnect-timing analysis and performance optimization. We begin with a brief discussion of the existing nominal delay metrics before proposing our methodology to extend these nominal metrics to include process variation.

Substantial work has been performed to develop accurate metrics for calculating delay and transition time in *RC* on-chip interconnects. Most of the existing metrics are moment-based, requiring computation of circuit moments that are then translated to delay and slew. The circuit moments of an *RC* tree can be computed efficiently by path tracing [19], [20]. The pth order circuit moment $(p > 1)$ of a node $i\,(m_p^i)$ in an *RC* tree can be expressed as

$$m_p^i = \sum_k \left(-R_{ik} C_k m_{p-1}^i\right). \tag{1}$$

Here, the summation is taken over all nodes other than the source node. C_k is the capacitance at node k and R_{ik} denotes the total overlap resistance in the unique paths from the source node to the nodes i and k.

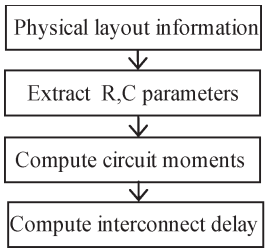

Moments	Delay Metrics	Slew Metrics
One	Elmore, Scaled Elmore	ln 9* Elmore
Two	D2M Weibull	S2M Scaled S2M
Three	h-gamma Lognormal	h-gamma Lognormal

Fig. 1. Moment-based-delay-modeling flow and some existing nominal delay and slew metrics as available in literature.

The existing delay modeling methodology and some of the existing moment-based metrics for delay and slew computation are summarized in Fig. 1. Some of the metrics shown in the table are of closed form (Elmore [21], D2M [22], S2M [23], Lognormal [24]) while others such as Weibull [25] and h-gamma [26] require lookup tables. In this paper, we focus only on closed-form metrics. An excellent summary of moment-based delay metrics can be found in [27].

In this section, we discuss a new approach to model interconnect-delay while considering variability in the physical dimensions. Once physical dimensions are mapped to electrical parameters, the resistances and capacitances become correlated random variables. Modeling these random variables as correlated pdfs and mapping these correlated pdfs to moments and then to a delay metric is very complex and does not provide any insight into the sensitivity of delay to variations in each physical dimension independently. In our methodology, we start by expressing electrical parameters as functions of changes in the physical parameters. During mapping of these electrical parameters to delay, we maintain this form in all intermediate steps and finally express delay directly as a function of changes in the physical parameters. The advantages of such a formulation are that it preserves all correlations and that it can be very useful in evaluating delay sensitivities due to changes in various physical dimensions. The formulation is also helpful in timing analysis as it allows delays to be easily summed while maintaining the correlations.

Our approach is based on the observation that the interconnect delay distribution with process variation considered is Gaussian. This implies that interconnect delay can be expressed as a linear function of variations in physical dimensions. This point allows us to simplify complex expressions by truncating them to their linear terms. The basic methodology of delay

Authorized licensed use limited to: University of Michigan Library. Downloaded on November 14, 2008 at 14:44 from IEEE Xplore. Restrictions apply.

computation remains the same as the conventional approach of Fig. 1. The steps in our approach are summarized below. Each of these steps is then discussed in detail in the following sections.

1) Express electrical parameters (resistances and capacitances) in terms of *changes* in physical dimensions.
2) Express moments in terms of electrical parameters and hence in terms of changes in physical dimensions.
3) Express interconnect delay as a function of moments and therefore in terms of changes in physical dimensions. Find mean and variance of delay distribution as a function of the statistics of variability in physical dimensions.

For simplicity, in the following discussion we consider variations only in metal width (W), metal thickness (T), and interlayer dielectric (ILD) thickness (H). In particular, we ignore material constant variations (dielectric constant and metal resistivity) and assume linewidth and spacing are perfectly negatively correlated, letting W be the independent variable. We explain our approach for these three dimensions; however, there is no restriction on the number of variables in our methodology. The approach can be easily extended to include other variation sources. We assume that the geometric variations are expressed as Gaussian distributions and that variation in one dimension is mutually independent with variations in other dimensions. We point out here that the assumption of independence may not hold for all processes and interconnect structures. However, in these cases, the problem can be simplified by transforming the dependent set of variables into uncorrelated variables by using the principal component analysis (PCA) technique [34]. A similar concept is employed by statistical static timing analysis approaches to handle spatial correlation [35], [36]. Once correlated variables are mapped into independent variables, the modeling methodology proposed in this paper can then be easily used by working on the transformed set of independent principal components.

A. Mapping Physical Dimensions to Electrical Parameters

To first order, delay through an interconnect can be expressed as the *RC* product of its resistance and capacitance. With any change in the physical dimensions of the wire, its resistance and capacitance also change, causing interconnect delay to fluctuate. In order to model the impact of variability on wire delay, we need to capture the effect of geometric variations on the electrical parameters. The change in electrical parameters due to variations in geometric dimensions can be captured by the simple linear approximation shown in (2)

$$\begin{aligned} R &= R_{\text{nom}} + a_1\Delta W + a_2\Delta T \\ C &= C_{\text{nom}} + b_1\Delta W + b_2\Delta T + b_3\Delta H. \end{aligned} \tag{2}$$

Here, R_{nom} and C_{nom} represent nominal resistance and capacitance values, computed when the wire dimensions are at their nominal or typical values. ΔW, ΔT, and ΔH represent the change in metal width, metal thickness, and ILD thickness, respectively. The coefficients a_i and b_i are the modeling coefficients in the linearized model. This linear approximation shows a high degree of accuracy for our purpose while remaining very simple to use. Linear models similar to (2) have been proposed in earlier works on interconnect variability [28]. In [28] the authors propose a methodology that requires a one-time nominal capacitance extraction after which lookup tables are used to calculate delta capacitances due to geometric parameter variations. In this paper, we use empirical capacitance modeling equations but any lookup table-based linear modeling approach can be used in a similar manner.

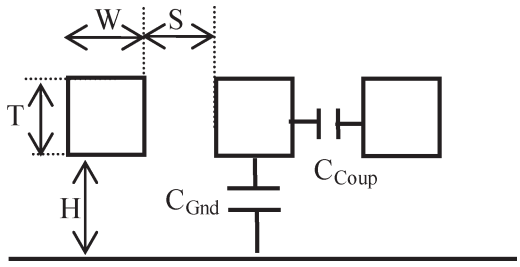

Fig. 2. Cross section of a generic interconnect structure.

For the simple structure shown in Fig. 2, the geometric parameters of interest are wire width (W), interwire spacing (S), ILD thickness (H) and metal thickness (T). For the middle line surrounded with two lines on the side, the line resistance and capacitances per unit length can be expressed using the following equations:

$$\begin{aligned} R &= \frac{\rho}{WT} \\ \frac{C_{Gnd}}{\varepsilon} &= \frac{W}{H} + 3.28\left(\frac{T}{T+2H}\right)^{0.023}\left(\frac{S}{S+2H}\right)^{1.16} \\ \frac{C_{Coup}}{\varepsilon} &= 1.064\frac{T}{S} + 3.28\left(\frac{T+2H}{T+2H+0.5S}\right)^{0.695} \\ &\quad + \left(\frac{W}{W+0.8S}\right)^{1.4148}\left(\frac{T+2H}{T+2H+0.5S}\right)^{0.804} \\ &\quad + 0.831\left(\frac{W}{W+0.8S}\right)^{0.055}\left(\frac{2H}{2H+0.5S}\right)^{3.542}. \end{aligned} \tag{3}$$

The capacitance expressions are taken from [29]. The linear modeling coefficients $a_{i'}$'s and b_i's can be readily computed by evaluating the partial derivatives of capacitance and resistance expressions given in (3) at the nominal point. The resistance and capacitance expressions in terms of changes in physical dimensions can now be written as

$$\begin{aligned} R &= R_{\text{nom}} + \left(\frac{\partial R}{\partial W}\right)_{\text{nom}}\Delta W + \left(\frac{\partial R}{\partial T}\right)_{\text{nom}}\Delta T \\ C &= C_{\text{nom}} + \left(\frac{\partial C}{\partial W}\right)_{\text{nom}}\Delta W + \left(\frac{\partial C}{\partial T}\right)_{\text{nom}}\Delta T \\ &\quad + \left(\frac{\partial C}{\partial H}\right)_{\text{nom}}\Delta H. \end{aligned} \tag{4}$$

We use the formulation of (4) in this paper. However, we point out that this formulation is not critical to our approach and any linearized models similar to (2) can be used in our

Authorized licensed use limited to: University of Michigan Library. Downloaded on November 14, 2008 at 14:44 from IEEE Xplore. Restrictions apply.

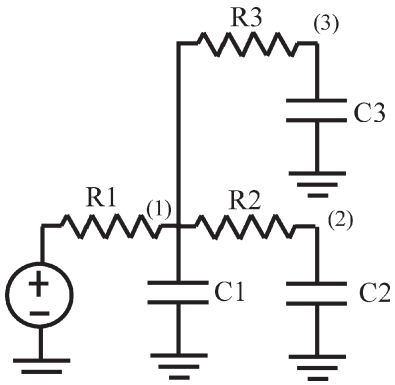

Fig. 3. Simple *RC* tree.

framework. We now discuss how these electrical parameters can be mapped to the moments.

B. Mapping Electrical Parameters to Moments

Once interconnect dimensions are mapped to the circuit parameters, the next step is the computation of circuit moments. For deterministic resistance and capacitance values in an *RC* tree, the circuit moments can be computed easily by path tracing as described earlier. However, with interconnect variability, the resistances and capacitances are now random variables. If changes in physical dimensions (ΔW, ΔT, etc.) are considered independent normal random variables, then the resistance and capacitance calculated using (2) are correlated normal random variables. This adds significant complexity in the moment-computation process, especially for higher order moments. We illustrate moment computation with variability for the simple *RC* tree example shown in Fig. 3.

The first moment at any node can be expressed as a function of resistances R_i's and capacitances C_i's. For example, the first moment at node 3 (without considering variability) in the above circuit is given by

$$m_1^3 = m_1(R_i, C_i) = -R_1(C_1 + C_2 + C_3) - R_3C_3. \quad (5)$$

With variations in physical dimensions, the resistances R_i and the capacitance C_i are linear functions of random variables (ΔW, ΔT, etc.).

$$\begin{aligned} R_i &= R_{i(\text{nom})} + R_{i(W)}\Delta W + R_{i(T)}\Delta T \\ C_i &= C_{i(\text{nom})} + C_{i(W)}\Delta W + C_{i(T)}\Delta T + C_{i(H)}\Delta H. \end{aligned} \quad (6)$$

Here, $R_{i(\text{nom})}$ and $C_{i(\text{nom})}$ are nominal resistance and capacitance, respectively. The coefficient $R_{i(W)}$ models the change in resistance R_i with a change in width ΔW. Similarly, other coefficients capture the delta resistance and delta capacitance with respect to each physical dimension. All such coefficients can be computed as discussed in Section II-A. Substituting R_i and C_i from (6) into (5) gives

$$\begin{aligned} m_1 = {} & m_{1(\text{nom})} + k_W\Delta W + k_T\Delta T + k_H\Delta H + k_{W^2}(\Delta W)^2 \\ & + k_{T^2}(\Delta T)^2 + k_{WT}(\Delta W\Delta T) + k_{WH}(\Delta W\Delta H) \\ & + k_{TH}(\Delta T\Delta H). \end{aligned} \quad (7)$$

Here, $m_{1(\text{nom})}$ is the first moment evaluated at nominal resistance $R_{i(\text{nom})}$ and nominal capacitance $C_{i(\text{nom})}$. We express this by the following notation:

$$m_{1(\text{nom})} = m_1\left(R_{i(\text{nom})}, C_{i(\text{nom})}\right). \quad (8)$$

The coefficients in (7) can be calculated by evaluating the first moment at different values of R's and C's. For example, the coefficient k_W^2 can be computed by calculating the first moment when all resistances and capacitances are replaced by the corresponding $R_{i(W)}$ and $C_{i(W)}$. The expressions for each coefficient in terms of first-moment computation are given in (9)

$$\begin{aligned} k_W &= m_1\left(R_{i(W)}, C_{i(\text{nom})}\right) + m_1\left(R_{i(\text{nom})}, C_{i(W)}\right) \\ k_{W^2} &= m_1\left(R_{i(W)}, C_{i(W)}\right) \\ k_T &= m_1\left(R_{i(T)}, C_{i(\text{nom})}\right) + m_1\left(R_{i(\text{nom})}, C_{i(T)}\right) \\ k_{T^2} &= m_1\left(R_{i(T)}, C_{i(T)}\right) \\ k_{WT} &= m_1\left(R_{i(W)}, C_{i(T)}\right) + m_1\left(R_{i(T)}, C_{i(W)}\right) \\ k_{WH} &= m_1\left(R_{i(W)}, C_{i(H)}\right) \\ k_{TH} &= m_1\left(R_{i(T)}, C_{i(H)}\right) \\ k_H &= m_1\left(R_{i(\text{nom})}, C_{i(H)}\right). \end{aligned} \quad (9)$$

Equation (7) shows the first-moment expression as a function of normal random variables representing variations in back-end physical dimensions. Equation (7) contains higher order terms and cross-product terms, thereby implying that the distribution of the first moment is not exactly Gaussian. However, experimentally, we find that the higher order terms are not significant and can be neglected without loss of accuracy (results are detailed later in this section). By neglecting higher order terms, the first-moment expression from (7) reduces to the following equation:

$$m_1 \cong m_{1(\text{nom})} + k_W\Delta W + k_T\Delta T + k_H\Delta H. \quad (10)$$

We can perform a similar analysis for the second moment. The second moment can be expressed as a function of resistances, capacitances, and the first moments. For example, the second moment at node 3 (without considering variability) for the circuit in Fig. 3 is given by

$$\begin{aligned} m_2^3 &= m_2(R_i, C_i, m_1^i) \\ &= -R_1\left(m_1^1C_1 + m_1^2C_2 + m_1^3C_3\right) - R_3\left(m_1^3C_3\right). \end{aligned} \quad (11)$$

With variations in physical dimensions, R_i's and C_i's can be replaced by their corresponding expressions from (6), and similarly, m_1's can be replaced by the expression given in (10). If we again keep only the linear terms, m_2 can be expressed as

$$m_2 \cong m_{2(\text{nom})} + A_W\Delta W + A_T\Delta T + A_H\Delta H. \quad (12)$$

Authorized licensed use limited to: University of Michigan Library. Downloaded on November 14, 2008 at 14:44 from IEEE Xplore. Restrictions apply.

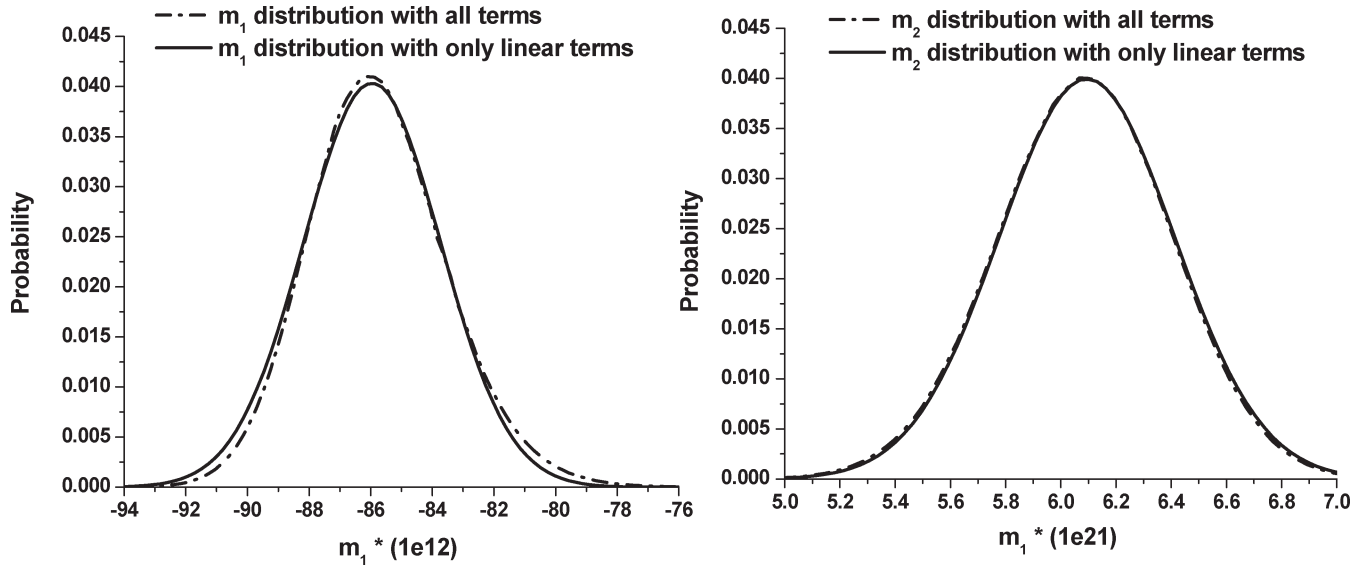

Fig. 4. First (left plot) and second (right plot) moment distributions with and without considering nonlinear terms.

Here, $m_{2(\mathrm{nom})}$ is the second moment evaluated at nominal resistance $R_{i(\mathrm{nom})}$, nominal capacitance $C_{i(\mathrm{nom})}$, and nominal first moment $m_{1(\mathrm{nom})}$. We express this using the following notation:

$$m_{2(\mathrm{nom})} = m_2(R_{i(\mathrm{nom})}, C_{i(\mathrm{nom})}, m_{1(\mathrm{nom})}). \tag{13}$$

The coefficients in (12) can be calculated by evaluating the second moment at different values of R's, C's, and m_1's

$$\begin{aligned} A_W =& m_2\left(R_{i(\mathrm{nom})}, C_{i(\mathrm{nom})}, k_W\right) \\ &+ m_2\left(R_{i(\mathrm{nom})}, C_{i(W)}, m_{1(\mathrm{nom})}\right) \\ &+ m_2\left(R_{i(W)}, C_{i(\mathrm{nom})}, m_{1(\mathrm{nom})}\right) \\ A_T =& m_2\left(R_{i(\mathrm{nom})}, C_{i(\mathrm{nom})}, k_T\right) \\ &+ m_2\left(R_{i(\mathrm{nom})}, C_{i(T)}, m_{1(\mathrm{nom})}\right) \\ &+ m_2\left(R_{i(T)}, C_{i(\mathrm{nom})}, m_{1(\mathrm{nom})}\right) \\ A_H =& m_2\left(R_{i(\mathrm{nom})}, C_{i(\mathrm{nom})}, k_H\right) \\ &+ m_2\left(R_{i(\mathrm{nom})}, C_{i(H)}, m_{1(\mathrm{nom})}\right). \end{aligned} \tag{14}$$

Here, k_W, k_T, and k_H can be computed as shown in (9). We again point out that (12) and (14) show only the linear coefficients. We can write a full expression of the second moment (similar to (7) for the first moment); however, we again find that the nonlinear terms are not significant and can be safely ignored.

To test the linearity assumption, we consider the simple configuration of Fig. 3. Nominal values for width and metal thickness are chosen to be 0.8 μm, while nominal ILD height was taken to be 0.55 μm. We consider a three-sigma tolerance of ± 0.1 μm in width and thickness and ± 0.05 μm in ILD thickness. We also assume that spacing is inversely correlated with width. Given these distributions of ΔW, ΔT, and ΔH, we plot the distributions of first and second moments at node 3 with and without the nonlinear terms. Fig. 4 shows that the two curves are nearly identical. The figure also shows that the distributions of moments are Gaussian, and hence, the linear approximations of (10) and (12) are extremely accurate.

We emphasize that truncating the moment expression to contain only the linear terms is not critical to our approach. The moments will finally be translated to a delay computation (discussed in Section II-C) and we will show that it is feasible to keep all nonlinear terms in that process. However, the number of terms grows significantly for higher order moments and retaining nonlinear terms does not provide appreciably better results. Therefore, we propose using truncated linear expressions of moments to simplify the analysis with negligible loss of accuracy.

To this point we have provided expressions for the first and second circuit moments as a function of random variables (ΔW, ΔT, etc.). We have also shown that the moments have Gaussian distributions and the complicated expressions of the moments can be safely truncated to contain only linear terms. This allows us to keep the expressions simple and tractable. Furthermore, we have demonstrated that the coefficients in the expressions of the moments can be easily computed in a manner similar to the nominal moment computation. We now turn our attention to mapping circuit moments to the delay metrics.

C. Mapping Moments to Delay Metrics

Once moments are expressed as functions of change in physical dimensions, the next step is to map the pdf of these moments to an interconnect-delay pdf. We begin by initially analyzing the simple first-moment-based $\ln 2 *$ Elmore (or scaled Elmore) metric and later, we show how the approach can be extended to more accurate higher order metrics such as D2M [22].

Authorized licensed use limited to: University of Michigan Library. Downloaded on November 14, 2008 at 14:44 from IEEE Xplore. Restrictions apply.

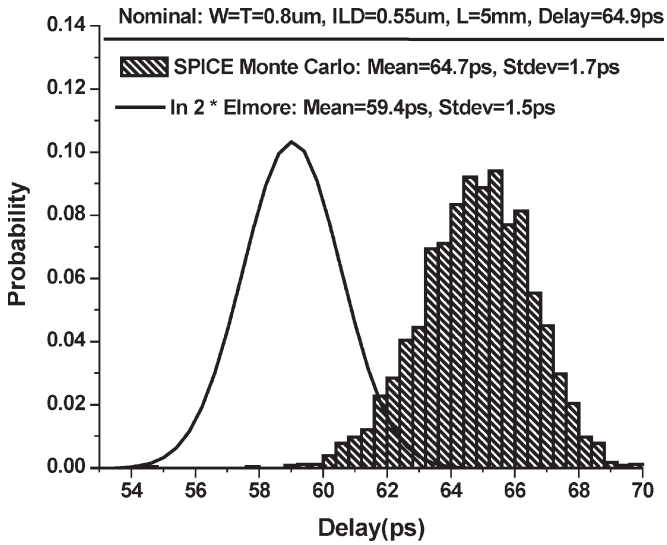

Fig. 5. Analytical delay distribution obtained using the statistical analysis of the scaled Elmore metric compared to Monte Carlo simulations. Nominal values (three-sigma tolerances) for metal width, thickness, and ILD height were 0.8 μm (± 0.1 μm), 0.8 μm (± 0.1 μm), and 0.55 μm (± 0.05 μm), respectively.

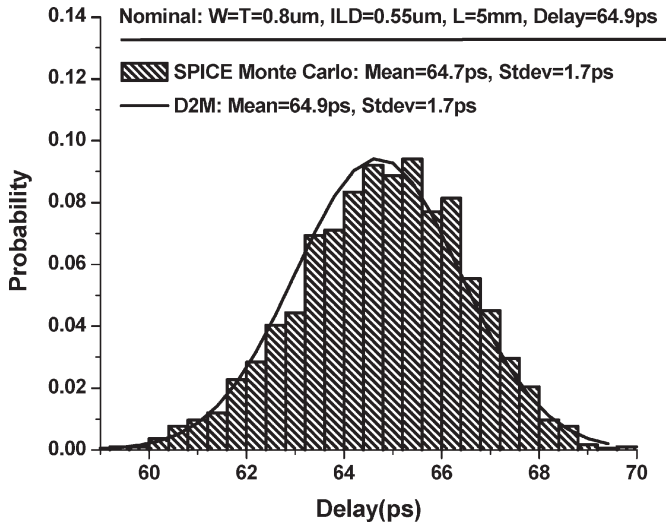

Fig. 6. Analytical delay distribution obtained using the statistical D2M metric compared to Monte Carlo simulations. Nominal values (three-sigma tolerances) for metal width, thickness, and ILD height were 0.8 μm (± 0.1 μm), 0.8 μm (± 0.1 μm), and 0.55 μm (± 0.05 μm), respectively.

We have already developed the expression for the first moment in (10). Hence, the scaled Elmore delay can be simply expressed as

$$\text{Delay} = -\ln 2 * \left[m_{1(\text{nom})} + k_W \Delta W + k_T \Delta T + k_H \Delta H\right]. \tag{15}$$

To test the above expression, we reconsider the test case used in Fig. 3. We perform 1000 Monte Carlo simulations and measure 50% delay in each case. Fig. 5 shows the distribution of delay measured from the simulations. The figure also shows the pdf for the delay generated using (15). Two important observations can be drawn from this figure: 1) a one moment-based metric is not sufficiently accurate for our purposes; and 2) the mean value of delay obtained using Monte Carlo simulations is very close to the nominal delay value. The implication of the first observation is that we need to incorporate higher order metrics to improve overall delay-estimation accuracy and the second observation indicates that the pdf of delay can be approximated using a Gaussian distribution.

We can also perform the above analysis by using the nontruncated expression of m_1. The delay will then be expressed as

$$\begin{aligned}\text{Delay} = -\ln 2 * \big[&m_{1(\text{nom})} + k_W \Delta W + k_{W^2} (\Delta W)^2 \\ &+ k_T \Delta T + k_{T^2} (\Delta T)^2 + k_{WT} (\Delta W \Delta T) \\ &+ k_{WH} (\Delta W \Delta H) + k_{TH} (\Delta T \Delta H) \\ &+ k_H \Delta H\big]. \end{aligned} \tag{16}$$

We found that the distribution computed with (16) matches that of (15) very closely. This further demonstrates that nonlinear terms can be ignored without loss of accuracy.

We have seen that first-order metrics are not sufficiently accurate such that the mean and variance calculated using (15) [or (16)] does not match well with Monte Carlo simulations. Among higher order metrics, we choose D2M for our analysis in this paper [22]. We explain our methodology for D2M, but the approach is independent of the metric and can be applied to any other closed-form delay metric.

Using D2M, the delay in terms of moments can be expressed as

$$\text{D2M} = \ln 2 * \frac{(m_{1(\text{nom})} + k_W \Delta W + k_T \Delta T + k_H \Delta H)^2}{\sqrt{m_{2(\text{nom})} + A_W \Delta W + A_T \Delta T + A_H \Delta H}}. \tag{17}$$

Analyzing the D2M expression in (17) is difficult, and hence, we can write a series expansion of the D2M expression and keep only the linear terms, as discussed earlier. The D2M expression can then be rewritten as

$$\text{D2M} \cong \ln 2 * \frac{(m_{1(\text{nom})})^2}{\sqrt{m_{2(\text{nom})}}} (1 + S_W \Delta W + S_T \Delta T + S_H \Delta H). \tag{18}$$

Here, S_W, S_T, and S_H can be calculated using

$$\begin{aligned} S_W &= \frac{2k_W}{m_{1(\text{nom})}} - \frac{A_W}{2m_{2(\text{nom})}} \\ S_T &= \frac{2k_T}{m_{1(\text{nom})}} - \frac{A_T}{2m_{2(\text{nom})}} \\ S_H &= \frac{2k_H}{m_{1(\text{nom})}} - \frac{A_H}{2m_{2(\text{nom})}}. \end{aligned} \tag{19}$$

We apply (18) to the same configuration as was used in Fig. 5. Fig. 6 shows the results as well as those from the Monte Carlo simulations.

Equation (18) is a simple linear function of ΔW, ΔT, and ΔH. If ΔW, ΔT, and ΔH are independent random variables with their mean values equal to zero and standard deviations

Authorized licensed use limited to: University of Michigan Library. Downloaded on November 14, 2008 at 14:44 from IEEE Xplore. Restrictions apply.

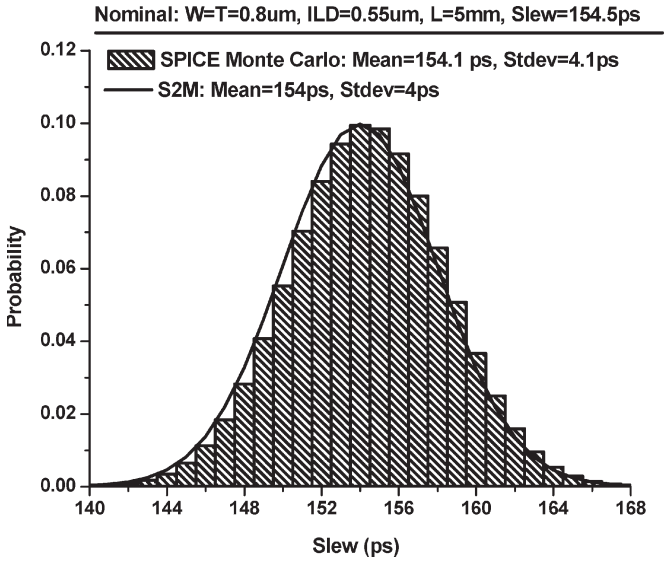

Fig. 7. Analytical slew distribution obtained using the statistical S2M metric compared to Monte Carlo simulations. Nominal values (three-sigma tolerances) for metal width, thickness, and ILD height were 0.8 μm (± 0.1 μm), 0.8 μm (± 0.1 μm), and 0.55 μm (± 0.05 μm), respectively.

of σ_W, σ_T, and σ_H, respectively, then the mean and standard deviation of delay in terms of the standard deviations in physical dimensions can be written as

$$E(\mathrm{D2M}) = \ln 2 * \frac{(m_{1(\mathrm{nom})})^2}{\sqrt{m_{2(\mathrm{nom})}}}$$

$$\mathrm{Stdev}(\mathrm{D2M}) = \ln 2 * \frac{(m_{1(\mathrm{nom})})^2}{\sqrt{m_{2(\mathrm{nom})}}} \times \sqrt{(S_W^2\sigma_W^2 + S_T^2\sigma_T^2 + S_H^2\sigma_H^2)}. \quad (20)$$

For the example of Fig. 6, the mean and standard deviation of the delay computed using (20) are 64.9 and 1.7 ps, respectively. These numbers match well with the 64.7 and 1.7 ps found using Monte Carlo simulations. We point out that the test case used to this point includes a rather wide line for which the variability is relatively small (three-sigma/mean for this linewidth is 12.5%). This results in only a small amount of delay variability. We will see in the results section that a net taken from an industrial-microprocessor design exhibits a quite substantial spread in interconnect delay using realistic uncertainty tolerances and the proposed models continue to perform well in such cases.

The above methodology can also be applied to slew computation. Fig. 7 compares the derived analytical slew distribution using the slew metric S2M [23] with Monte Carlo simulations for the same test case. The figure shows that the proposed methodology works equally well for slew as for delay.

The advantage of (18) lies in its simplicity, making it useful in evaluating delay sensitivity to variation in a particular physical dimension. This equation preserves the closed-form nature of the nominal delay metrics and can be used to calculate the standard deviation of interconnect delays in an efficient manner. In Section V, we test our approach on a variety of test cases. The overall modeling flow is summarized below.

Given the following information:

1) a physical net;
2) process variation in geometric dimensions.

Perform the following steps for computing interconnect delay distribution.

1) Extract nominal resistance and capacitance of the net and compute their linear coefficients [see (2)].
2) Evaluate first moment repeatedly and compute k_W, k_T, and k_H [see (9)].
3) Evaluate second moment repeatedly and compute A_W, A_T, and A_H [see (14)].
4) Compute S_W, S_T, and S_H [see (19)].
5) Model delay distribution as Gaussian distribution [see (18)].

D. Extension to Ramp Inputs

The statistical-delay and slew-modeling methodology proposed in the previous section can be easily extended to include ramp-input waveforms. We use the probability density function extension to ramp inputs (PERI) metric [30] for estimating the delay and slew of the output given a saturated ramp input. Under this formulation, delay (D) and slew (S) are formulated as

$$D = (1-\alpha)\mu + \alpha M$$

$$\alpha = \left(\frac{2m_2 - m_1^2}{2m_2 - m_1^2 + \frac{T_\mathrm{R}^2}{12}}\right)^{\frac{5}{2}}$$

$$\mu = -m_1 \quad M = \ln(2)\cdot\frac{m_1^2}{\sqrt{m_2}}$$

$$S = \sqrt{\left(\ln^2(9)\cdot(2m_2 - m_1^2) + 0.8^2\cdot T_\mathrm{R}^2\right)}. \quad (21)$$

Here, m_1 and m_2 are the first and second circuit moments, μ is the Elmore delay [21], M is the D2M delay metric [22], and T_R is the rise time of the input signal.

To include the impact of process variations in the above model, circuit moments m_1 and m_2 are replaced by the statistical expressions given in (10) and (12), and the resulting equations are further simplified by applying Taylor-series expansions. Finally, all higher order terms in $\Delta W, \Delta T$, and ΔH are removed. The final expressions for D and S obtained in this manner are given by

$$D \cong D_\mathrm{nom} + (1-\alpha_\mathrm{nom})\Delta\mu - \Delta\alpha\cdot\mu_\mathrm{nom} + \Delta\alpha\cdot M_\mathrm{nom} + \alpha_\mathrm{nom}\Delta M$$

$$\Delta\alpha = \frac{5}{12}\cdot\alpha\cdot T_\mathrm{R}^2\cdot\frac{(\Delta m_2 - m_1\Delta m_1)}{(2m_2 - m_1^2)\cdot\left(2m_2 - m_1^2 + \frac{T_\mathrm{R}^2}{12}\right)}$$

$$\Delta M = -M_\mathrm{nom}\cdot\left(\frac{2\Delta m_1}{m_1} + \frac{\Delta m_2}{2m_2}\right)$$

$$S \cong S_\mathrm{nom}\cdot\left(1 + \frac{\ln^2(9)\cdot(\Delta m_2 - m_1\Delta m_1)}{S_\mathrm{nom}^2}\right). \quad (22)$$

Authorized licensed use limited to: University of Michigan Library. Downloaded on November 14, 2008 at 14:44 from IEEE Xplore. Restrictions apply.

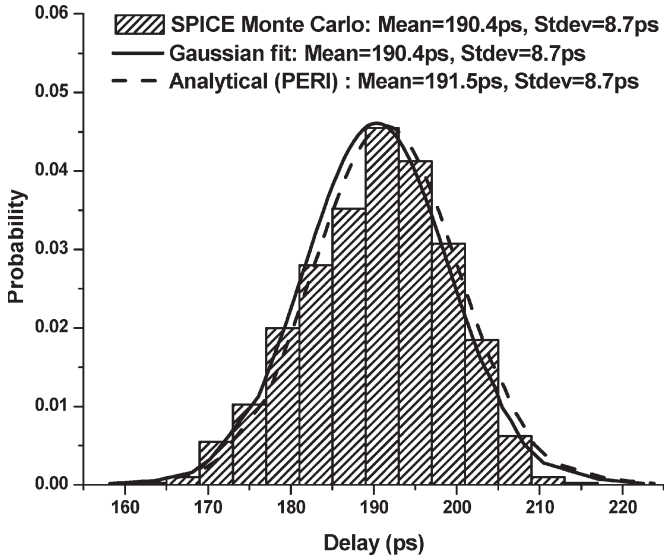

Fig. 8. Analytical delay distribution for saturated ramp input obtained using the statistical PERI method compared to Monte Carlo simulations. The Gaussian-fit curve shows Gaussian fitting to the HSPICE mean and standard deviation. Nominal values (three-sigma tolerances) for metal width, thickness, and ILD height were 0.5 μm (13%), 0.4 μm (16%), and 0.3 μm (19%), respectively.

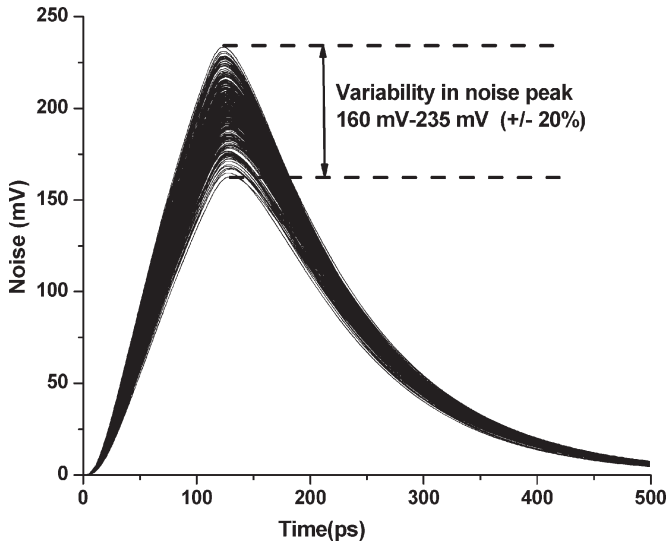

Fig. 9. Crosstalk-noise waveforms as obtained by Monte Carlo simulations. Nominal values (three-sigma tolerances) for metal width, thickness, and ILD height were 0.4 μm (25%), 0.75 μm (21%), and 0.3 μm (17%), respectively. Nominal interwire spacing was 0.45 μm and it was inversely correlated with width.

Here, $\Delta m_1 (= k_W \Delta W + k_T \Delta T + k_H \Delta H)$ and $\Delta m_2 (= A_W \Delta W + A_T \Delta T + A_H \Delta H)$, representing variability terms in the first and second moments, can be computed in a manner discussed in the previous section.

In order to verify this result, we compare the analytical model with SPICE-based Monte Carlo simulations. The probability plots for one random test case are shown in Fig. 8. For this test case, the values for W, T, and H were randomly chosen to be 0.5, 0.4, and 0.3 μm, respectively, and their 3-σ variabilities were selected to be 13%, 16%, and 19%, respectively. The figure shows histograms obtained using Monte Carlo simulations and compares them to two Gaussian distributions. The first Gaussian pdf was obtained by fitting a Gaussian distribution to the mean and standard deviation obtained using Monte Carlo simulations. A good fit of this Gaussian pdf to Monte Carlo simulations verified the linearity (Gaussian) assumption. The second Gaussian pdf was obtained by using the analytical model proposed in this section. The mean and standard deviation of delay computed using the analytical model were 190.4 and 8.7 ps, respectively. These numbers match well with the values of 191.5 and 8.7 ps found using Monte Carlo SPICE simulations.

III. Statistical Modeling of Static Noise

In this section, we discuss the impact of process variation on static crosstalk noise in coupled *RC* interconnects. Static noise is defined as the noise pulse induced on a quiet victim net due to the switching of neighboring aggressors. Static noise can result in functional failures due to false switching of the victim line. For the first order, the magnitude of static noise is directly proportional to the ratio of coupling capacitance to total ground capacitance. This causes the noise magnitude to be very sensitive to variations in metal width and interwire spacing, and small variations in these dimensions can result in large fluctuations in the noise peak. To demonstrate this claim, we consider a simple coupled *RC*-interconnect test case. The width (W), thickness (T), spacing (S), and ILD layer thickness (H) for the interconnect lines were randomly chosen to be 0.4, 0.75, 0.45, and 0.3 μm, respectively. Moreover, the variation in W, T, and H were taken to be 25%, 21%, and 17% of the nominal values, respectively (recall that we consider W and S to be perfectly inversely correlated). Fig. 9 shows the spread of noise waveforms obtained using HSPICE Monte Carlo simulations. The figure shows that for this test case, the noise peak varies from approximately 160 to 235 mV, thereby implying that variation in noise due to process variation can be significant and should be modeled accurately.

We use the nominal static-noise-peak model proposed in [13] for our analysis. This model approximates victim and aggressor *RC*-distributed interconnects by a six-node symmetric template as shown in Fig. 10. By solving this template, the noise peak induced on the victim line is given by

$$\text{Noise}_{\text{peak}} = \frac{t_X}{t_{\text{R}}} \cdot \frac{\left(1 - \text{e}^{-\frac{t_{\text{R}}}{t_V}}\right)^p}{\left(1 - \text{e}^{-\frac{t_{\text{R}}}{t_A}}\right)^q} \tag{23}$$

where

$$t_X = C_X \cdot (R_V + R_{VL}); \quad q = \frac{t_V}{t_V - t_A}; \quad p = \frac{\text{t}_{\text{A}}}{t_V - t_A}$$

$$t_V = C_{VL} \cdot R_V + (C_{VM} + C_X) \cdot (R_V + R_{VL}) + C_{VR} \cdot (R_V + R_{VL} + R_{VR})$$

$$t_A = C_{AL} \cdot R_A + (C_{AM} + C_{\text{veff}} + C_{\text{reff}}) \cdot (R_A + R_{AL}).$$

Authorized licensed use limited to: University of Michigan Library. Downloaded on November 14, 2008 at 14:44 from IEEE Xplore. Restrictions apply.

Also, $t_{\rm R}$ is the rise time for the saturated-ramp-input signal at the aggressor line. $C_{\rm reff}$ and $C_{\rm veff}$ are the effective capacitances for the right half of the aggressor and the victim line, respectively, as discussed in [13].

In the presence of process variations, all resistances and capacitances shown in Fig. 10 become correlated random variables. These random variables are modeled as linear functions of changes in physical dimensions [see (6)]. These resistances and capacitances can then be substituted in the t_X, t_V, and t_A expressions. These expressions are then simplified by neglecting higher order terms of ΔW, ΔT, and ΔH. This assumption is highly accurate because ΔW, ΔT, and ΔH are small quantities, and hence, higher order terms containing multiplications of these quantities can be safely ignored. This approximation also preserves linearity with respect to the process variations. Under these assumptions, t_X, t_V, and t_A are given by

$$\begin{aligned} t_X &= (T_X + \Delta T_X) = T_X + x_w \Delta W + x_T \Delta T + x_H \Delta H \\ t_V &= (T_V + \Delta T_V) = T_V + \nu_w \Delta W + \nu_T \Delta T + \nu_H \Delta H \\ t_A &= (T_A + \Delta T_A) = T_A + a_w \Delta W + a_T \Delta T + a_H \Delta H. \end{aligned} \tag{24}$$

Here, T_X, T_V, and T_A are nominal values. The results from (24) can now be substituted in the $\text{Noise}_{\rm peak}$ expression of (23). However, this results in a highly complex function with various nonlinear terms appearing in a very complicated manner. This new expression is stepwise reduced by using Taylor-series expansions. At each reduction step, higher order product terms containing ΔW, ΔT, and ΔH are ignored. Finally, we arrive at an expression for $\text{Noise}_{\rm peak}$ that is a linear function of ΔW, ΔT, and ΔH. This expression is given by

$$\begin{aligned} \text{Noise}_{\rm peak} &\cong (\text{Noise}_{\rm peak,nom} + \Delta\text{Noise}_{\rm peak}) \\ \Delta\text{Noise}_{\rm peak} &= \text{Noise}_{\rm peak,nom} \cdot \left(\frac{\Delta T_X}{T_X} + M \Delta T_V + N \Delta T_A \right) \\ M &= \frac{\rm B}{T_V - T_A} \cdot \ln \left(\frac{1 - {\rm e}^{-\frac{T_{\rm R}}{T_V}}}{1 - {\rm e}^{-\frac{T_{\rm R}}{T_A}}} \right) \\ &\quad + \frac{\rm A \cdot T_R}{T_A^2} \cdot \frac{{\rm e}^{-\frac{T_{\rm R}}{T_A}}}{\left(1 - {\rm e}^{-\frac{T_{\rm R}}{T_A}} \right)} \\ N &= -\frac{\rm A}{T_V - T_A} \cdot \ln \left(\frac{1 - {\rm e}^{-\frac{T_{\rm R}}{T_V}}}{1 - {\rm e}^{-\frac{T_{\rm R}}{T_A}}} \right) \\ &\quad - \frac{\rm B \cdot T_R}{T_V^2} \cdot \frac{{\rm e}^{-\frac{T_{\rm R}}{T_V}}}{\left(1 - {\rm e}^{-\frac{T_{\rm R}}{T_V}} \right)} \\ A &= \frac{T_A}{T_V - T_A} \\ B &= \frac{T_V}{T_V - T_A}. \end{aligned} \tag{25}$$

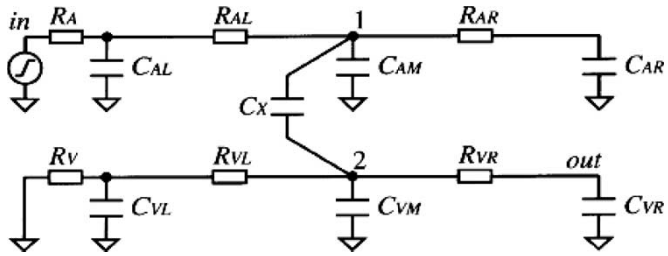

Fig. 10. Six-node circuit template for coupling noise estimation as used in [13].

The above formulation is linear with respect to variations in physical dimensions, thereby implying that for normal distribution functions for W, T, and H, the distribution of $\text{Noise}_{\rm peak}$ is also normal. To verify the statistical noise-peak model proposed in (25) with respect to HSPICE Monte Carlo simulations, we consider a pair of 15-segment *RC* interconnects and apply a saturated ramp input at the aggressor line with a rise time of 110 ps. The width, thickness, spacing, and ILD thickness are randomly taken to be 0.55, 0.44, 0.4, and 0.3 μm, respectively. The 3-σ normal variabilities in the abovementioned parameters are also randomly chosen as 14%, 30%, and 15% of the nominal values, respectively. Again, spacing is considered to be inversely related to width (pitch is constant). Our model is based on the assumption that under normal distributions of process variations, the static-peak-noise distribution is also Gaussian. To test this assumption, we look at the quantile–quantile (q–q) plot of the noise-peak distribution obtained from HSPICE simulations and compare it with the analytical model. The q–q plot is a graphical technique for determining if two data sets come from populations with a common distribution. A q–q plot is a plot of the quantiles of the first data set against the quantiles of the second data set, where a quantile indicates the fraction (or percentage) of points below the given value. Fig. 11 shows this comparison and demonstrates that the q–q plots of HSPICE simulations and the analytical model match very well. The figure also shows that the distributions fall along a 45° reference line, thus validating the proposed model. Fig. 12 shows these results using histograms and Gaussian pdfs. Once again, it is clear from this figure that noise-peak distribution is Gaussian and the mean and variance of this distribution as obtained using the analytical model match well with Monte Carlo results.

The impact of noise on functional failures is typically characterized by noise-immunity curves. In this section, we proposed a method for the statistical modeling of crosstalk-noise peak under process variations. Under linearity assumption, the approach can be extended to model other parameters such as noise width or area in a similar manner. These noise parameters (peak and area) should then be compared against statistical noise-immunity curves to fully characterize the impact of process variations on functional failures. In this work, we focus on noise-peak modeling, but future work will extend this model to consider this effect.

IV. Dynamic-Delay Modeling

Dynamic delay is defined as the signal delay on the victim line when both the aggressor and the victim switch

Authorized licensed use limited to: University of Michigan Library. Downloaded on November 14, 2008 at 14:44 from IEEE Xplore. Restrictions apply.

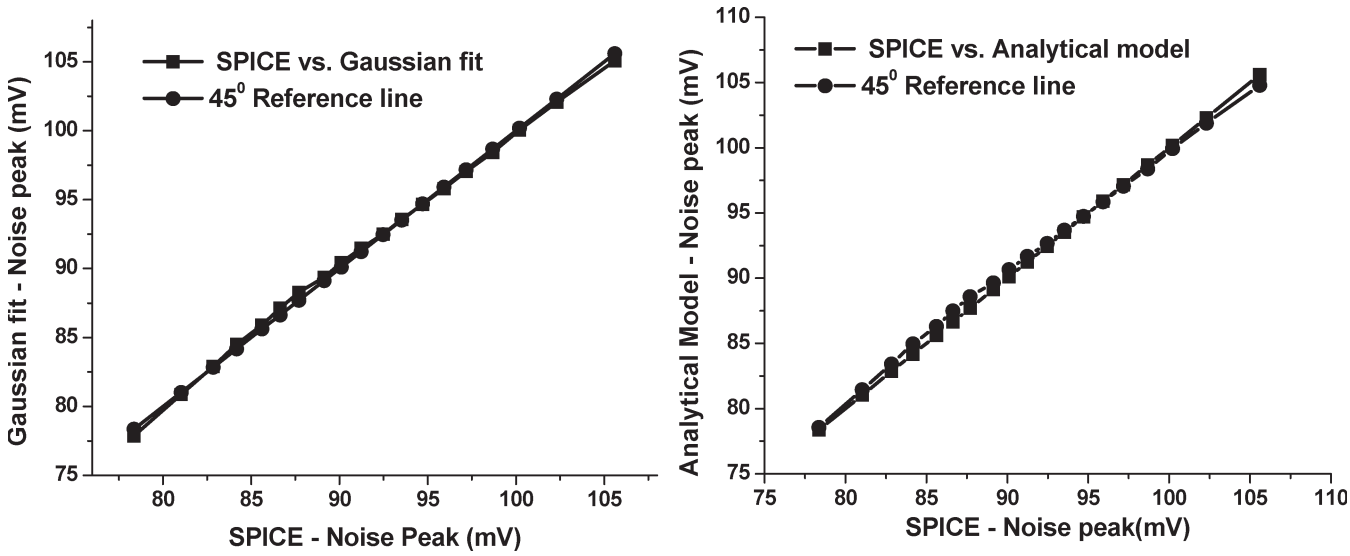

Fig. 11. q–q plots for noise peak: (Left) HSPICE results versus Gaussian distribution (with same mean and standard deviation as obtained from SPICE simulations) with 45° reference line. (Right) SPICE result versus the analytical model with 45° reference line. Nominal values (three-sigma tolerances) for metal width, thickness, and ILD height were 0.55 μm (14%), 0.44 μm (30%), and 0.3 μm (15%), respectively. Nominal interwire spacing was 0.4 μm and it was inversely correlated with width.

simultaneously. It is well known that an adjacent switching aggressor can either slow down or speed up a victim depending on its switching polarity with respect to the victim. The victim becomes slower in the case of out-of-phase switching and faster due to in-phase switching. The delay push-out during out-of-phase switching is a major concern due to the possibility of setup-time failures, and hence, must be accounted for in order to ensure correct operation of the circuit. In this section, we discuss dynamic-delay modeling with and without process variations.

A. Nominal-Delay-Noise Model

Dynamic delay can be modeled by the superposition of the static-noise waveform on the isolated victim waveform. In [33], and subsequently in [16], previous authors have used this principle to describe dynamic delay. In [16], static noise is approximated by a linear ramp followed by a decaying exponential term. The isolated victim waveform is modeled as an exponential function. The two waveforms are superimposed and the new 50%-delay point is computed analytically. However, some problems with this approach are the fact that the waveform approximations are not highly accurate and some parameters required for waveform modeling are extracted through the curve fitting of HSPICE results. This model predicts dynamic delay as a function of the relative switching times of the aggressor and victim wires. It is often the case that the designer is only interested in the worst case delay change and this value can be accurately computed by considering the worst case alignment of victim-and-aggressor switching [18]. In this section, we first develop a new dynamic-delay model that uses accurate waveform modeling along with worst case alignment to compute for worst case dynamic delay.

Our dynamic-delay model is based on the superposition principle, as in [16] and [33]. Hence, accurate estimation of dynamic delay requires accurate modeling of both the static noise and the isolated victim switching waveforms. Static noise can be modeled using the approach discussed in the previous section. However, modeling of the entire victim switching waveform is a separate (and complex) problem. A Weibull function-based waveform model was recently proposed in [31]. The Weibull function is given by

$$y = 1 - \mathrm{e}^{-\left(\frac{t}{\beta}\right)^{\alpha}}. \tag{26}$$

In order to fully characterize the Weibull function, we match the delay and the slew of the actual output with the above expression. If we denote the 50% V_{DD} crossing time

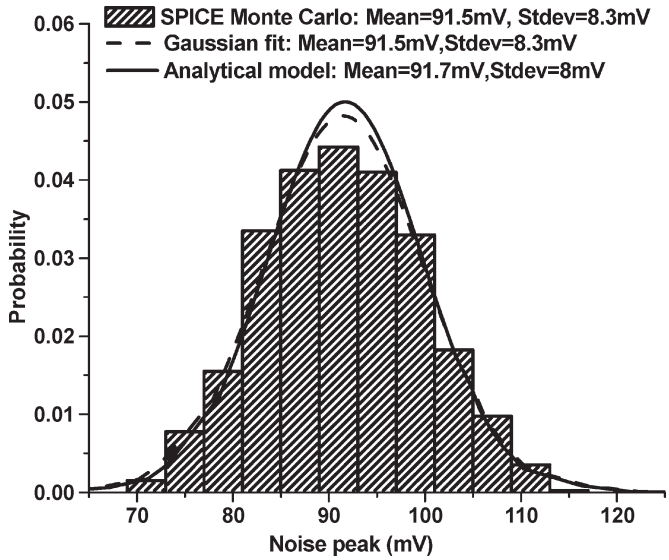

Fig. 12. Analytical noise-peak distribution compared to Monte Carlo simulations. The Gaussian-fit curve shows Gaussian fitting to the HSPICE mean and standard deviation. Nominal values (three-sigma tolerances) for metal width, thickness, and ILD height were 0.55 μm (14%), 0.44 μm (30%), and 0.3 μm (15%), respectively. Nominal interwire spacing was 0.4 μm and it was inversely correlated with width.

Authorized licensed use limited to: University of Michigan Library. Downloaded on November 14, 2008 at 14:44 from IEEE Xplore. Restrictions apply.

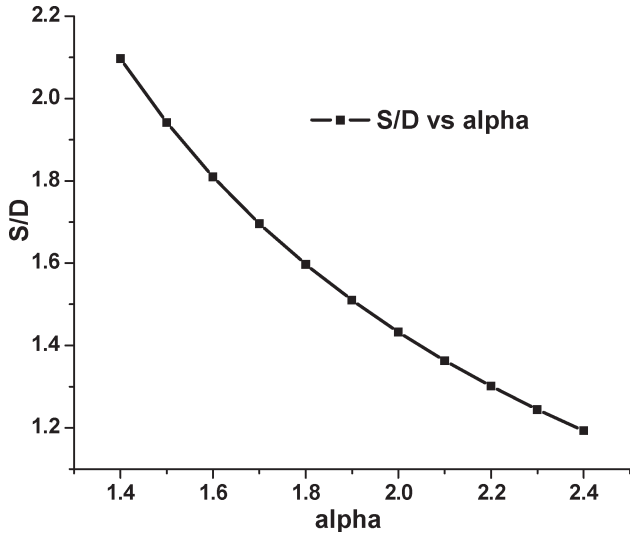

Fig. 13. Slew/Delay (S/D) as a function of Weibull parameter α. A second-order-polynomial fitting is used to express S/D in terms of α.

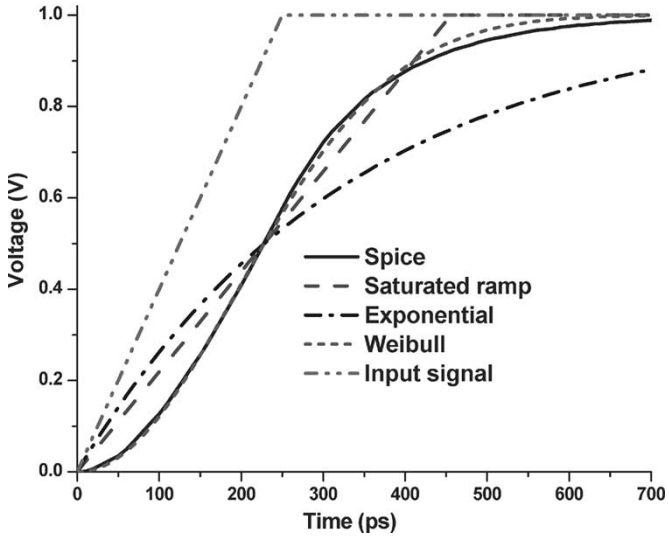

Fig. 14. Output waveform of an *RC* circuit under ramp input. The figure shows actual HSPICE results and various analytical approximations of the waveform.

of the output waveform as D and 10%–90% slew as S. Then, we have

$$D = \beta \cdot (\ln 2)^{\frac{1}{\alpha}}$$
$$S = \beta \cdot \left((\ln 10)^{\frac{1}{\alpha}} - \left(\ln \frac{10}{9} \right)^{\frac{1}{\alpha}} \right). \tag{27}$$

The values for D and S can be computed analytically using any of the existing delay and slew metrics [22]–[27]. We use the PERI metric (21) for estimating delay and slew for a saturated ramp input. Now, these values of D and S can be used in (27) to solve for the Weibull parameters α and β. However, the problem is that the equation set in (27) can only be solved using numerical techniques. We therefore make the following simplifications to solve (27) in a closed-form manner, which is in keeping with the goals of this work.

By dividing S by D, we obtain

$$\frac{S}{D} = \frac{\left((\ln 10)^{\frac{1}{\alpha}} - \left(\ln \frac{10}{9} \right)^{\frac{1}{\alpha}} \right)}{(\ln 2)^{\frac{1}{\alpha}}}. \tag{28}$$

The above expression of S/D is plotted for a practical range of α (1.4–2.4) as obtained through simulations over a large set of test cases. Fig. 13 shows this plot. This graph can now be fitted by a simple second-order polynomial as follows:

$$\frac{S}{D} = 0.5392\alpha^2 - 2.9274\alpha + 5.124. \tag{29}$$

Equation (29) can be easily solved to compute α in terms of S/D. The value of α thus obtained is then substituted in (27) to estimate β. The values of α and β computed in this manner can now be used in (26) to fully characterize the Weibull waveform model of an isolated victim.

To verify this theory, we compare the analytical result with HSPICE simulations. Fig. 14 shows that the Weibull waveform obtained using the above method fits an actual waveform very accurately. The figure also shows that simple-ramp or exponential expressions are highly inaccurate, and hence, using them for dynamic-delay prediction will result in highly erroneous results.

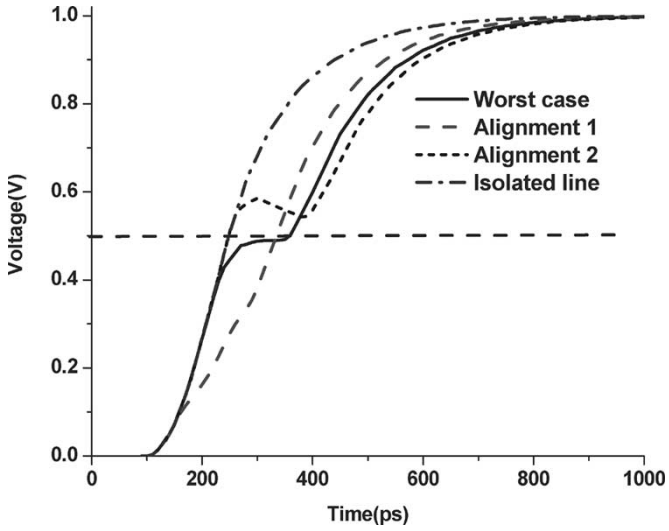

Fig. 15. Worst case alignment of noise peak that results in maximum delay degradation. Alignment 1 and 2 refer to the cases when noise peaks occur before and after this worst case alignment, respectively. These alignments have smaller impact on 50% switching time as compared to the worst case alignment.

Once the waveforms are modeled accurately, the next step in dynamic-delay modeling is to superimpose the static noise on the isolated victim delay waveform. This superposition should be done in a manner that results in maximum delay shift to model the worst case switching behavior. This is achieved by aligning aggressor and victim switching such that the time when the static noise reaches its maximum value $(\text{Noise}_{\text{peak}})$ is matched to the time when the isolated victim delay waveform crosses the $(0.5V_{\text{DD}} + \text{Noise}_{\text{peak}})$ value [18], [33]. This condition is explained in Fig. 15. In Fig. 15, alignment 1 and 2 refer to the cases when noise peaks occur before and after the time at which the isolated line waveform crosses $(0.5V_{\text{DD}} + \text{Noise}_{\text{peak}})$ voltage level.

Authorized licensed use limited to: University of Michigan Library. Downloaded on November 14, 2008 at 14:44 from IEEE Xplore. Restrictions apply.

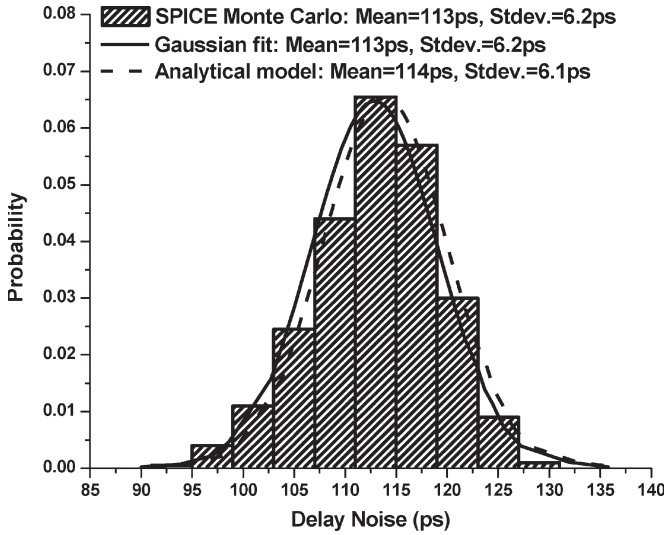

Fig. 16. Analytical coupling-induced dynamic-delay distribution compared to Monte Carlo simulations. The Gaussian-fit curve shows Gaussian fitting to the HSPICE mean and standard deviation. Nominal values (three-sigma tolerances) for metal width, thickness, and ILD height were 0.65 μm (23%), 0.5 μm (11%) and 0.26 μm (11%), respectively. Nominal interwire spacing was 0.4 μm and it was inversely correlated with width.

For the Weibull-waveform model, the above condition results in the following equation for 50% switching time (t_{50}) of the victim waveform:

$$1 - \mathrm{e}^{-\left(\frac{t_{50}}{\beta}\right)^{\alpha}} = \frac{1}{2} + \mathrm{Noise}_{\mathrm{peak}}. \tag{30}$$

The above expression of t_{50} can now be used to solve for worst case dynamic delay (x_{delay})

$$x_{\mathrm{delay}} = \beta \ln^{\frac{1}{\alpha}} \left(\frac{1}{0.5 - \mathrm{Noise}_{\mathrm{peak}}} \right) - \frac{T_{\mathrm{R}}}{2}. \tag{31}$$

The x_{delay} thus computed gives the final expression for estimating the worst case dynamic delay due to simultaneous switching of aggressor and victim wires. The overall modeling flow is summarized below.

For a given coupled *RC* network, perform the following steps to compute worst case dynamic delay.

1) Compute the slew (S) and the delay (D) of an isolated victim line by (21).
2) Model the victim waveform by the Weibull model. Compute Weibull parameters α and β using (27) and (29).
3) Compute for the value of noise peak $\mathrm{Noise}_{\mathrm{peak}}$ using (23).
4) Use worst case victim-and-aggressor alignment to calculate worst case dynamic delay using (31).

B. Statistical-Delay-Noise Model

In the previous section, we discussed a methodology to estimate worst case dynamic delay in coupled *RC* interconnects. For the statistical modeling of delay noise, we begin with this nominal dynamic-delay-modeling methodology. Based on the above modeling flow, the first step is to compute slew (S) and delay (D) under process variations. These can be easily computed by using (22) as discussed in Section II-D. The next step is to compute statistical expressions for α, β, and $\mathrm{Noise}_{\mathrm{peak}}$. Under a linear assumption, α, β, and $\mathrm{Noise}_{\mathrm{peak}}$ can be replaced with

$$\begin{aligned} \alpha &= \alpha_{\mathrm{nom}} + \Delta\alpha \\ \beta &= \beta_{\mathrm{nom}} + \Delta\beta \\ \mathrm{Noise}_{\mathrm{peak}} &= \mathrm{Noise}_{\mathrm{peak,nom}} + \Delta\mathrm{Noise}_{\mathrm{peak}}. \end{aligned} \tag{32}$$

Expressions for $\Delta\mathrm{Noise}_{\mathrm{peak}}$ have already been given in (25). $\Delta\alpha$ and $\Delta\beta$ are formulated by substituting expressions for S and D from (22) into (27) and (29). After truncating to retain only linear terms, the final reduced formulation for α and β is given by (33), shown at the bottom of the page. Here, ΔD and ΔS represent variability in delay and slew as obtained from (22).

Now, we can substitute α, β, and $\mathrm{Noise}_{\mathrm{peak}}$ in (31). Once again, under the Gaussian (linear) assumption, the final expression for dynamic delay can be expressed as

$$\begin{aligned} x_{\mathrm{delay}} \cong & \left(\frac{1}{0.5 - N_{\mathrm{peak}}} \right) \\ & \times \left(1 + \frac{\Delta\beta}{\beta} - \frac{\Delta N_{\mathrm{peak}}}{\alpha \cdot (0.5 - N_{\mathrm{peak}}) \cdot \ln(0.5 - N_{\mathrm{peak}})} \right. \\ & \left. - \frac{\Delta\alpha}{\alpha^2} \ln\left(-\ln(0.5 - N_{\mathrm{peak}})\right) \right) - \frac{T_{\mathrm{R}}}{2}. \end{aligned} \tag{34}$$

Equations (31) and (34) are our final results for nominal and statistical dynamic-delay modeling. To verify these equations, we compare our results against Monte Carlo simulations in a manner similar to the static-noise example. The probability plots and q–q plots for one randomly selected test case are shown in Figs. 16 and 17, respectively. The width, thickness, spacing, and ILD thickness for this arbitrarily chosen test case are taken as 0.65, 0.5, 0.4, and 0.26 μm, respectively, and 3-σ variations for the above parameters were 23%, 11%, and 11% of their nominal values, respectively. Once again, it is clear from these figures that the Gaussian approximation is accurate and the analytical mean and standard deviation

$$\begin{aligned} \alpha &\cong \alpha_{\mathrm{nom}} - \frac{2.1568 \times \left(\Delta S - \frac{S}{D} \cdot \Delta D\right)}{(4 \times 0.5392) \cdot D \cdot \sqrt{(2.9274)^2 - 4 \times 0.5392 \times \left(5.124 - \frac{S}{D}\right)}} \\ \beta &\cong \beta_{\mathrm{nom}} + \frac{\left(\Delta D + \frac{D}{\alpha^2} \ln(\ln 2) \cdot \Delta\alpha\right)}{(\ln 2)^{\frac{1}{\alpha}}} \end{aligned} \tag{33}$$

Authorized licensed use limited to: University of Michigan Library. Downloaded on November 14, 2008 at 14:44 from IEEE Xplore. Restrictions apply.

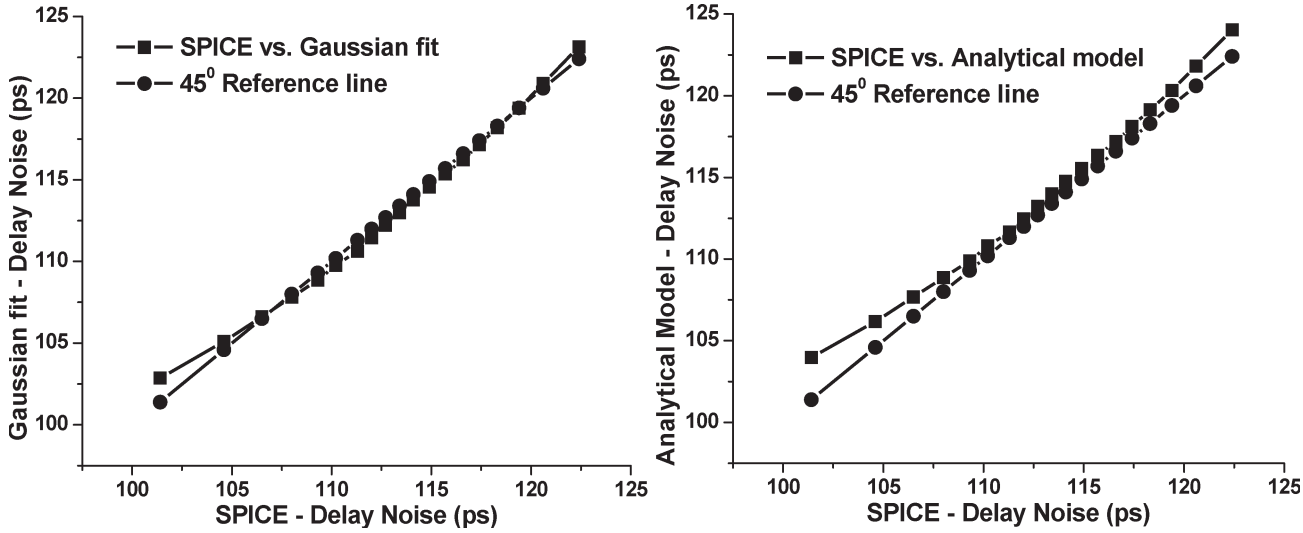

Fig. 17. q–q plots for dynamic delay: (Left) HSPICE results versus Gaussian distribution (with same mean and standard deviation as obtained from SPICE simulations) with 45° reference line. (Right) SPICE result versus analytical model with 45° reference line. Nominal values (three-sigma tolerances) for metal width, thickness, and ILD height were 0.65 μm (23%), 0.5 μm (11%), and 0.26 μm (11%), respectively. Nominal interwire spacing was 0.4 μm and it was inversely correlated with width.

calculated under this assumption match well with SPICE simulations. A good match in the nominal (mean) values of the dynamic delay (113 ps by HSPICE as compared to 114 ps by the model) verifies the nominal dynamic-delay model as given in (31). Similarly, a good match in the standard deviation values (6.2 ps by HSPICE compared to 6.1 ps by the model) verifies the proposed statistical dynamic-delay model as given by (34).

V. Experimental Results

In this section, we test our methodology on various test cases. In each of the previous sections, we first proposed an analytical model and then we checked its accuracy on a simple example. In this section, we test the proposed models extensively over a variety of examples and report error statistics by comparing our models with Monte Carlo HSPICE simulations on a large set of test cases. All simulations were performed using 130-nm technology with 1-V supply.

A. Variational-Delay-Metric Verification

In this section, we verify the variational-delay model proposed in Section II. First, we test the Gaussian (and hence the linearity) assumption when the variations in physical dimensions are large. We choose a simple line with nominal metal width and thickness of 0.6 μm and nominal ILD thickness of 0.45 μm. We consider three-sigma variations of 30% in all three dimensions, which is slightly larger than the expected levels of back-end process variability [1], [32]. Fig. 18 compares the delay distribution using our approach with Monte Carlo simulations. The figure shows that, even with large variations in geometric dimensions, the delay distribution remains Gaussian and the proposed model captures its mean and variance very accurately.

To further quantify error incurred due to the linearity assumption, we consider the test case of Fig. 18 and sweep three-sigma percentage variation in physical dimensions from 5% to 50% of the nominal value. For each three-sigma variation point, we calculate the standard deviation of the interconnect delay distribution using the proposed analytical statistical D2M model and compare it with Monte Carlo simulations. Fig. 19 shows percentage error in standard deviation as a function of three-sigma percentage variation in geometric dimensions. The figure shows that the error increases with an increase in variability. This is because the linearity assumption becomes less accurate for larger values of variability. However, the figure shows that for this test case, the proposed model (and hence, the linearity assumption) provides good results ($< 10\%$ error) for sufficiently large levels of back-end process variation ($< 30\%$).

For the next experiment, we revisit the test case discussed in Figs. 5–7. Modeling this 5-mm line using 30 identical

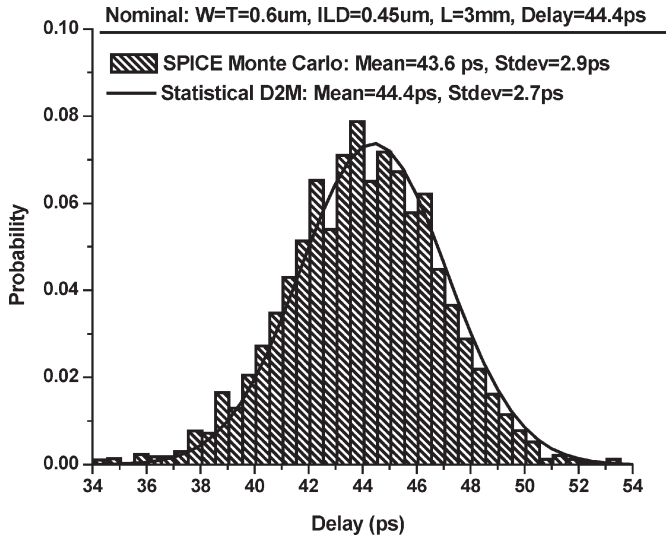

Fig. 18. Analytical delay distribution obtained using statistical D2M metric compared to Monte Carlo simulations. Nominal values (three-sigma tolerances) for metal width, thickness, and ILD height were 0.6 μm (30%), 0.6 μm (30%), and 0.45 μm (30%), respectively.

Authorized licensed use limited to: University of Michigan Library. Downloaded on November 14, 2008 at 14:44 from IEEE Xplore. Restrictions apply.

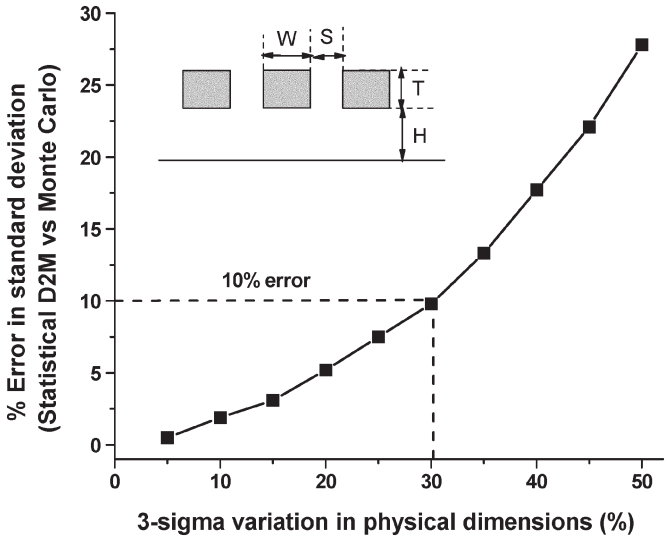

Fig. 19. Error in statistical D2M model as a function of percentage variation in physical dimensions.

TABLE I
COMPARING ANALYTICAL MEAN AND STANDARD DEVIATION OF DELAY DISTRIBUTION WITH SPICE MONTE CARLO SIMULATIONS FOR VARIOUS NODES IN A SIMPLE 30-SEGMENT LINE

Node	Nom Delay (ps) (SPICE)	Mean (ps)		Stdev (ps)	
		SPICE	Model	SPICE	Model
10	20.9	20.8	28.2	0.56	0.73
15	41.1	40.9	43.4	1.1	1.12
20	55	54.8	55.2	1.46	1.43
25	62.5	62.3	62.6	1.67	1.63
30	64.9	64.7	64.9	1.71	1.69

segments, we look at the various nodes along the line and compute their distributions. Table I compares the mean and standard deviation found using Monte Carlo simulations with the proposed model. The table shows that the model works well across all nodes. Node 10 shows a relatively large error in the mean and variance computation, but this error is primarily due to the error in D2M in nominal delay calculation for near-end nodes and not the statistical component of the model. Table I also shows the nominal delay computed using HSPICE. We observe here that the means computed using Monte Carlo simulations are very close to the nominal delays for all the nodes, thereby implying that the Gaussian assumption is applicable for intermediate nodes as well.

We also generated a large set of random test cases by varying nominal physical dimensions and their three-sigma variabilities. Nominal linewidths and thicknesses were allowed to vary from 0.4 to 0.8 μm, while nominal ILD thickness could take values between 0.25 and 0.55 μm. For each test case, the three-sigma variability in each of the three physical dimensions was randomly chosen to be between 10% and 30% of the nominal value. Table II shows the average error in mean and standard deviation of delay for 2900 test cases compared to Monte Carlo simulations. The table also shows the error bins. The three-sigma variation in delay for this set of test cases ranged from 5% to 34% of the mean. This implies that even with the reverse trends shown by resistance and capacitance

TABLE II
AVERAGE ERROR IN MEAN AND STANDARD-DEVIATION ESTIMATION OF INTERCONNECT-DELAY DISTRIBUTION COMPARED TO MONTE CARLO SIMULATIONS

2900 testcases	Mean (Delay)	Stdev (Delay)
Avg. Error	1.2%	3.8%
Error Bins	Mean(Delay)	Stdev(Delay)
<1%	31.7%	15.7%
<2%	92.3%	33.9%
<5%	100%	75.5%

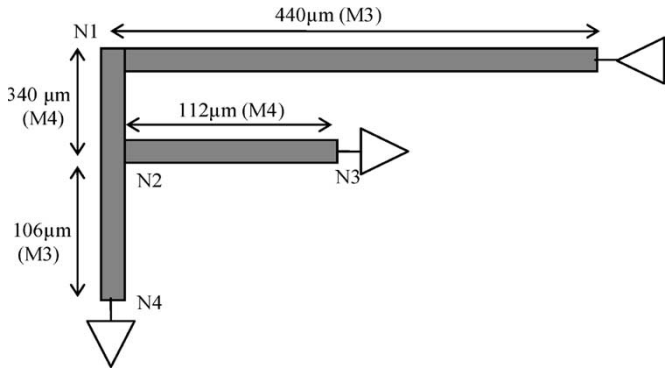

Fig. 20. Topology of a physical net taken from an industrial design.

TABLE III
COMPARING ANALYTICAL MEAN AND STANDARD DEVIATION OF DELAY DISTRIBUTION WITH SPICE MONTE CARLO SIMULATIONS FOR VARIOUS NODES OF THE NET SHOWN IN FIG. 19

Node	Nom Delay (ps) (SPICE)	Mean (ps)		Stdev (ps)	
		SPICE	Model	SPICE	Model
N1	16.1	16.1	17.7	1.83	1.9
N2	26.1	26.1	26.1	3.3	3.2
N3	28.1	28	28.1	3.5	3.47
N4	28.6	28.5	28.6	3.64	3.58

for a given change in physical dimensions, the delay variability due to back-end process tolerances can be large and should be modeled accurately.

As a final experiment, we tested the new approach on an actual net taken from an industrial design. The routed topology of the net is shown in Fig. 20. The three-sigma tolerances in the physical dimensions were taken from relevant process technology. We examined the delay distributions at nodes N1 to N4 along the net and compared them to our approach. The results in Table III indicate that the model works very well. Note that the spread in the delay distribution is quite large for this industrial example, pointing to a need for the proposed type of variational interconnect modeling.

B. Static-Noise Peak and Dynamic-Delay-Model Verification

In this section, we first verify the statistical-noise model proposed in Section III against HSPICE Monte Carlo simulations. We compare our results for 2300 random test cases generated by varying nominal physical dimensions and their three-sigma variabilities. Nominal linewidth, thickness, and spacing were randomly chosen between 0.4 and 0.8 μm. ILD thickness was

Authorized licensed use limited to: University of Michigan Library. Downloaded on November 14, 2008 at 14:44 from IEEE Xplore. Restrictions apply.

TABLE IV
AVERAGE ERROR IN MEAN AND STANDARD-DEVIATION ESTIMATION OF CROSSTALK-NOISE PEAK AND COUPLING-INDUCED WORST CASE DYNAMIC DELAY COMPARED TO MONTE CARLO SIMULATIONS

2300 testcases	**Mean (Noise peak)**	**Stdev (Noise peak)**
Avg. Error.	2.7%	3.7%
	Mean (Dynamic Delay)	**Stdev (Dynamic Delay)**
Avg. Error	2.6%	12.4%

varied between 0.25 and 0.55 μm. For each test case, the three-sigma variability in each of the three physical dimensions was randomly chosen to be between 10% and 30% of the nominal. Spacing was assumed to be in inverse correlation with width, i.e., pitch (linewidth + spacing) was assumed to be constant. In addition to these terms, the rise time of the input signal (saturated ramp) was also randomly chosen to be between 70 and 500 ps. Table IV shows the average error in the mean and the standard deviation for these 2300 test cases compared to Monte Carlo simulations. The table shows that the model works well with average error values of 2.7% and 3.7%, respectively, for the mean and standard deviation of the noise peak. For these test cases, nominal noise peak varied between 50 and 330 mV and the three-sigma variation in noise peak ranged from 3% to 40%.

Finally, to test the new dynamic-delay model [(31) and (34)], we compare our results with the worst case dynamic delay computed using SPICE simulations for the above set of randomly generated *RC* interconnect line configurations. Table IV shows the average error of the mean and standard deviation for these test cases compared to Monte Carlo simulations. The table shows that the models proposed in Sections IV-A and IV-B work very well. The overall three-sigma variation ranged from 3% to 30% for the test cases under consideration, thereby implying that variability in dynamic delay can be significant and must be modeled accurately.

VI. CONCLUSION

In this work, we describe simple techniques for efficient variational modeling of VLSI interconnects for statistical physical-design optimizations. First, we developed a methodology to extend popular closed-form moment-based delay and slew metrics to consider back-end process variation. These variational delay metrics are based on the use of linearized models of electrical parameters (*R*, *C*) that capture uncertainty in process parameters such as linewidth, metal thickness, and ILD thickness (W, T, H). These models are then used to compute moments using known path-tracing techniques—a key point is that only terms linear with the random variables (W, T, H) were found to be necessary to ensure good accuracy. These variation-aware moments were then used in accurate delay and slew metrics such as D2M and S2M to capture the distribution of interconnect timing. We demonstrate good accuracy in the mean and standard deviation of the resulting interconnect delay distribution for a number of test cases (1.2% and 3.8% average error, respectively, for 2900 randomly generated test cases). We also tested the approach on a large industrial net and found significant variability in the interconnect delay, motivating the need for the newly developed variational-delay-modeling approach. We also proposed an analytical model to estimate the mean and the variance of coupling noise and dynamic delay in the presence of process variations. The proposed noise models are also based on the assumption that distribution functions of crosstalk noise and delay can be approximated as normal random variables, thereby allowing us to simplify the models by truncating complex expressions to retain only linear terms. In the process, we developed a new model for worst case coupling-induced delay estimation. The proposed model uses accurate Weibull waveform modeling along with the worst case victim/aggressor alignment to estimate worst case delay change in a closed-form manner. We compare our approach with SPICE and show that the mean and standard deviation computed by the proposed model match well with simulations. Due to its efficiency and accuracy, the proposed techniques can be very useful in statistical noise-related physical-design optimizations.

REFERENCES

[1] S. R. Nassif, "Modeling and analysis of manufacturing variations," in *Proc. Custom Integrated Circuits Conf.*, San Diego, CA, 2001, pp. 223–228.
[2] K. Keutzer and M. Orshansky, "From blind certainty to informed uncertainty," in *Proc. Int. Workshop Timing Issues Specification and Synthesis Digital Systems (TAU)*, Monterey, CA, 2002, pp. 37–41.
[3] S. R. Nassif, "Delay variability: Sources, impact and trends," in *Proc. Int. Solid State Circuits Conf.*, San Francisco, CA, 2000, pp. 368–369.
[4] K. A. Bowman, S. G. Duvall, and J. D. Meindl, "Impact of die-to-die and within-die parameter fluctuations on the maximum clock frequency distribution for gigascale integration," *IEEE J. Solid-State Circuits*, vol. 37, no. 2, pp. 183–190, Feb. 2002.
[5] Z. Lin, C. Spanos, L. Milor, and Y. Lin, "Circuit sensitivity to interconnect variation," *IEEE Trans. Semicond. Manuf.*, vol. 11, no. 4, pp. 557–568, Nov. 1998.
[6] Y. Liu, S. R. Nassif, L. T. Pileggi, and A. J. Strojwas, "Impact of interconnect variations on the clock skew of a gigahertz microprocessor," in *Proc. Design Automation Conf.*, Los Angeles, CA, 2000, pp. 168–171.
[7] Y. Liu, L. T. Pileggi, and A. J. Strojwas, "Model order reduction of RC(L) interconnect including variational analysis," in *Proc. Design Automation Conf.*, New Orleans, LA, 1999, pp. 201–206.
[8] A. Odabasioglu, M. Celik, and L. T. Pileggi, "PRIMA: Passive reduced-order interconnect macromodeling algorithm," in *Proc. Int. Conf. Computer Aided Design*, San Jose, CA, 1997, pp. 58–65.
[9] T. Sakurai, "Closed-form expressions for interconnection delay, coupling and crosstalk in VLSIs," *IEEE Trans. Electron Devices*, vol. 40, no. 1, pp. 118–124, Jan. 1993.
[10] A. Vittal, L. Chen, M. Marek-Sadowska, K. P. Wang, and S. Yang, "Crosstalk in VLSI interconnections," *IEEE Trans. Comput.-Aided Des. Integr. Circuits Syst.*, vol. 18, no. 2, pp. 1817–1824, Dec. 1999.
[11] A. Devgan, "Efficient coupled noise estimation for on-chip interconnects," in *Proc. Int. Conf. Computer-Aided Design*, San Jose, CA, 1997, pp. 147–153.
[12] E. Acar, A. Odabasioglu, M. Celik, and L. Pileggi, "S2P: A stable 2-pole RC delay and coupling noise metric for IC interconnects," in *Proc. Great Lakes Symp. VLSI*, Ann Arbor, MI, 1999, pp. 60–63.
[13] L. Ding, D. Blaauw, and P. Mazumder, "Accurate crosstalk noise modeling for early signal integrity," *IEEE Trans. Comput.-Aided Des. Integr. Circuits Syst.*, vol. 22, no. 5, pp. 627–634, May 2003.
[14] L. H. Chen and M. Marek-Sadowska, "Closed-form crosstalk noise metrics for physical design applications," in *Proc. Design Automation and Test Eur. Conf.*, Paris, France, 2002, pp. 812–819.
[15] A. B. Kahng, S. Muddu, and E. Sarto, "On switch factor based analysis of coupled RC interconnects," in *Proc. Design Automation Conf.*, Los Angeles, CA, 2000, pp. 79–84.
[16] T. Sato, Y. Cao, K. Agarwal, D. Sylvester, and C. Hu, "Bidirectional closed-form transformation between on-chip coupling noise waveforms and interconnect delay-change curves," *IEEE Trans. Comput.-Aided Des. Integr. Circuits Syst.*, vol. 22, no. 5, pp. 560–572, May 2003.

Authorized licensed use limited to: University of Michigan Library. Downloaded on November 14, 2008 at 14:44 from IEEE Xplore. Restrictions apply.

[17] S. Bhardwaj, S. B. K. Vrudhula, and D. Blaauw, "Estimation of signal arrival times in the presence of delay noise," in *Proc. Int. Conf. Computer Aided Design*, San Jose, CA, Nov. 2002, pp. 418–422.
[18] D. Blaauw, S. Sirichotiyakul, C. Oh, R. Levy, V. Zolotov, and J. Zuo, "Driver modeling and alignment for worst-case delay noise," *IEEE Trans. Very Large Scale Integr. (VLSI) Syst.*, vol. 11, no. 2, pp. 157–166, Apr. 2003.
[19] Q. Yu and E. S. Kuh, "Exact moment matching model of transmission lines and application to interconnect delay estimation," *IEEE Trans. Very Large Scale Integr. (VLSI) Syst.*, vol. 3, no. 2, pp. 311–322, Jun. 1995.
[20] C. L. Ratzlaff, N. Gopal, and L. T. Pillage, "RICE: Rapid interconnect circuit evaluator," in *Proc. Design Automation Conf.*, San Francisco, CA, 1991, pp. 555–560.
[21] W. C. Elmore, "The transient response of damped linear networks with particular regard to wideband amplifiers," *J. Appl. Phys.*, vol. 19, no. 1, pp. 55–63, Jan. 1948.
[22] C. J. Alpert, A. Devgan, and C. Kashyap, "A two moment RC delay metric for performance optimization," in *Proc. Int. Symp. Physical Design*, San Diego, CA, 2000, pp. 69–74.
[23] K. Agarwal, D. Sylvester, and D. Blaauw, "Simple metrics for slew rate of RC circuits based on two circuit moments," in *Proc. Design Automation Conf.*, Anaheim, CA, 2003, pp. 950–953.
[24] C. J. Alpert, F. Liu, C. Kashyap, and A. Devgan, "Delay and slew metrics using the lognormal distribution," in *Proc. Design Automation Conf.*, Anaheim, CA, 2003, pp. 382–385.
[25] F. Liu, C. Kashyap, and C. J. Alpert, "A delay metric for RC circuits based on the Weibull distribution," in *Proc. Int. Conf. Computer Aided Design*, San Jose, CA, 2002, pp. 620–624.
[26] T. Lin, E. Acar, and L. Pileggi, "*h*-gamma: An RC delay metric based on a gamma distribution approximation to the homogenous response," in *Proc. Int. Conf. Computer-Aided Design*, San Jose, CA, 1998, pp. 19–25.
[27] L. T. Pileggi, "Timing metrics for physical design of deep submicron technologies," in *Proc. Int. Symp. Physical Design*, Monterey, CA, 1998, pp. 28–33.
[28] V. Mehrotra, S. Nassif, D. Boning, and J. Chung, "Modeling the effects of manufacturing variation on high-speed microprocessor interconnect performance," presented at the *IEEE Electron Devices Meetings*, pp. 767–770, San Jose, CA, 1998.
[29] J. Chern, J. Huang, L. Arledge, P. Li, and P. Yang, "Multilevel metal capacitance models for CAD design synthesis systems," *IEEE Electron Device Lett.*, vol. 13, no. 1, pp. 32–34, Jan. 1992.
[30] C. V. Kashyap, C. J. Alpert, F. Liu, and A. Devgan, "Closed-form expressions for extending step delay and slew metrics to ramp inputs for RC trees," *IEEE Trans. Comput.-Aided Des. Integr. Circuits Syst.*, vol. 23, no. 4, pp. 509–516, Apr. 2004.
[31] C. Amin, F. Dartu, and Y. I. Ismail, "Weibull based analytical waveform model," in *Proc. Int. Conf. Computer Aided Design*, San Jose, CA, Nov. 2003, pp. 161–168.
[32] S. Nakagawa, private communication, UbiTech Inc.
[33] F. Dartu and L. T. Pileggi, "Calculating worst-case gate delays due to dominant capacitive coupling," in *Proc. ACM/IEEE Design Automation Conf.*, Anaheim, CA, 1997, pp. 46–51.
[34] D. F. Morrison, *Multivariate Statistical Methods*. New York: McGraw-Hill, 1976.
[35] H. Chang and S. S. Sapatnekar, "Statistical timing analysis considering spatial correlations using a single PERT-like traversal," in *Proc. Int. Conf. Computer-Aided Design*, San Jose, CA, 2003, pp. 621–625.
[36] C. Visweswariah, K. Ravindran, K. Kalafala, S. Walker, and S. Narayan, "First-order incremental block-based statistical timing analysis," in *Proc. Design Automation Conf.*, San Diego, CA, 2004, pp. 331–336.

Kanak Agarwal (S'01–M'05) received the B.E. degree in electrical engineering from the Birla Institute of Technology and Science, Pilani, India, in 2000 and the M.S. and Ph.D. degrees in electrical engineering from University of Michigan, Ann Arbor, in 2003 and 2004, respectively. His dissertation work focused on various nanometer-design issues such as leakage-power estimation and minimization, impact of process variation on performance and power, and on-chip interconnect modeling.

Currently, he is with the IBM Research Lab, Austin, TX. His current research is focused on high-speed and low-power circuit design, and statistical characterization and modeling of process variations. He is also interested in exploring novel device structures and circuit families that can advance the life of scaling beyond conventional CMOS.

Mridul Agarwal, photograph and biography not available at the time of publication.

Dennis Sylvester (S'96–M'97–SM'04) received the B.S. degree in electrical engineering (*summa cum laude*) from the University of Michigan, Ann Arbor, in 1995 and the M.S. and Ph.D. degrees in electrical engineering from University of California, Berkeley, in 1997 and 1999, respectively. His dissertation research was recognized with the 2000 David J. Sakrison Memorial Prize as the Most Outstanding Research in the UC–Berkeley Electrical Engineering and Computer Sciences (EECS) Department.

He worked at Hewlett–Packard Laboratories, Palo Alto, CA, from 1996 to 1998. After working in the Advanced Technology Group of Synopsys, Mountain View, CA, he is now an Associate Professor of Electrical Engineering at the University of Michigan, Ann Arbor. He has published numerous articles in his field of research, which includes low-power circuit design and design-automation techniques, design for manufacturability, and on-chip interconnect modeling. He also serves as a Consultant and Technical Advisory Board Member for several electronic-design automation firms in these areas.

Dr. Sylvester received an National Science Foundation (NSF) Career Award, the 2000 Beatrice Winner Award at the International Solid-State-Circuits Conference (ISSCC), the 2004 IBM Faculty Award, and several Best Paper awards and nominations. He is the recipient of the 2003 Association for Computing Machinery (ACM) Special Interest Group on Design Automation (SIGDA) Outstanding New Faculty Award, the 1938E Award from the College of Engineering for teaching and mentoring, and the Henry Russel Award, which is the highest award given to faculty at the University of Michigan. He has served on the Technical Program Committee of numerous design-automation and circuit-design conferences, including General Chair of the 2003 ACM/IEEE System-Level Interconnect Prediction (SLIP) Workshop and 2005 ACM/IEEE Workshop on Timing Issues in the Synthesis and Specification of Digital Systems (Tau). He is an Associate Editor for IEEE TRANSACTIONS ON VERY LARGE SCALE INTEGRATION SYSTEMS. In addition, he helped define the circuit and physical-design roadmap as a member of the International Technology Roadmap for Semiconductors (ITRS) U.S. Design Technology Working Group from 2001 to 2003. He is a member of ACM, American Society of Engineering Education, and Eta Kappa Nu.

David Blaauw (M'94) received the B.S. degree in physics and computer science from Duke University, Durham, NC, in 1986, the M.S. degree in computer science from the University of Illinois, Urbana, in 1988, and the Ph.D. degree in computer science from the University of Illinois, Urbana, in 1991.

He worked at IBM Corporation as a Development Staff Member until August 1993. From 1993 to August 2001, he worked for Motorola, Inc., Austin, TX, where he was the Manager of the High Performance Design Technology Group. Since August 2001, he has been on the faculty at the University of Michigan, Ann Arbor, as an Associate Professor. His work has focused on very-large-scale-integration (VLSI) design and computer-aided design (CAD) with particular emphasis on circuit design and optimization for high-performance and low-power designs.

Dr. Blaauw was the Technical Program Chair and General Chair for the International Symposium on Low Power Electronic and Design in 1999 and 2000, respectively, and was the Technical Program Cochair and member of the Executive Committee of the ACM/IEEE Design Automation Conference in 2000 and 2001.

Authorized licensed use limited to: University of Michigan Library. Downloaded on November 14, 2008 at 14:44 from IEEE Xplore. Restrictions apply.